Bioorganic Chemistry 110 (2021) 104795

Contents lists available at ScienceDirect

Bioorganic Chemistry

journal homepage: www.elsevier.com/locate/bioorg

Identification of new 3-phenyl-1*H*-indole-2-carbohydrazide derivatives and their structure–activity relationships as potent tubulin inhibitors and anticancer agents: A combined *in silico*, *in vitro* and synthetic study

Rungroj Saruengkhanphasit [a], Chutikarn Butkinaree [b,c], Narittira Ornnork [d], Kriengsak Lirdprapamongkol [d], Worawat Niwetmarin [a], Jisnuson Svasti [d], Somsak Ruchirawat [a,e,f], Chatchakorn Eurtivong [a,f,*]

[a] Program in Chemical Sciences, Chulabhorn Graduate Institute, Chulabhorn Royal Academy, Bangkok 10210, Thailand
[b] Program in Applied Biological Sciences, Chulabhorn Graduate Institute, Chulabhorn Royal Academy, Bangkok 10210, Thailand
[c] National Omics Center, National Science and Technology Development Agency, Pathum Thani 12120, Thailand
[d] Laboratory of Biochemistry, Chulabhorn Research Institute, Bangkok 10210, Thailand
[e] Laboratory of Medicinal Chemistry, Chulabhorn Research Institute, Bangkok 10210, Thailand
[f] Center of Excellence on Environmental Health and Toxicology (EHT), Commission on Higher Education (CHE), Ministry of Education, Bangkok 10400, Thailand

ARTICLE INFO

Keywords:
Virtual screening
CDRUG
3-phenyl-1*H*-indole-2-carbohydrazide
Anticancer agents
Tubulin polymerisation
Molecular docking

ABSTRACT

Virtual screening of commercially available molecular entities by using CDRUG, structure-based virtual screening, and similarity identified eight new derivatives of 3-phenyl-1*H*-indole-2-carbohydrazide with anti-proliferative activities. The molecules were tested experimentally for inhibition of tubulin polymerisation, which revealed furan-3-ylmethylene-3-phenyl-1*H*-indole-2-carbohydrazide (**27a**) as the most potent candidate. Molecule **27a** was able to induce G2/M phase arrest in A549 cell line, similar to other tubulin inhibitors. Synthetic modifications of **27a** were focussed on small substitutions on the furan ring, halogenation at R_1 position and alteration of furyl connectivity. Derivatives **27b**, **27d** and **27i** exhibited the strongest tubulin inhibition activities and were comparable to **27a**. Bromine substitution at R_1 position showed most prominent anticancer activities; derivatives **27b-27d** displayed the strongest activities against HuCCA-1 cell line and were more potent than doxorubicin and the parent molecule **27a** with IC_{50} values <0.5 μM. Notably, **27b** with a 5-methoxy substitution on furan displayed the strongest activity against HepG2 cell line ($IC_{50} = 0.34$ μM), while **27d** displayed stronger activity against A549 cell line ($IC_{50} = 0.43$ μM) compared to doxorubicin and **27a**. Fluorine substitutions at the R_1 position tended to show more modest anti-tubulin and anticancer activities, and change of 2-furyl to 3-furyl was tolerable. The new derivatives, thiophenyl **26**, displayed the strongest activity against A549 cell line ($IC_{50} = 0.19$ μM), while 1-phenylethylidene **21b** and **21c** exhibited more modest anticancer activities with unclear mechanisms of action; **26** and **21c** demonstrated G2/M phase arrest, but showed weak tubulin inhibitory properties. Molecular docking suggests the series inhibit tubulin at the colchicine site, in agreement with the experimental findings. The calculated molecular descriptors indicated that the molecules obey Lipinski's rule which suggests the molecules are drug-like structures.

1. Introduction

Tubulin is a protein monomer of polymeric microtubules that contribute to key functions in cell physiology: formation of mitotic spindle fibres, intracellular transport, maintenance of cell shape, and cell motility [1]. During mitosis, duplicated chromosomes separate towards opposing poles along the mitotic spindle fibres before the two daughter cells are formed [2]. Due to its key role in mitosis, tubulin has been designated as a key biomolecular target for an array of anticancer agents [1,2]. These agents typically modulate microtubule dynamics and are broadly characterised as either microtubule-destabilising or stabilising agents, which inhibit and promote tubulin polymerisation,

* Corresponding author at: Program in Chemical Sciences, Chulabhorn Graduate Institute, Chulabhorn Royal Academy, 906 Kamphaeng Phet 6, Talat Bang Khen, Lak Si, Bangkok 10210, Thailand.
E-mail address: chatchakorn@cgi.ac.th (C. Eurtivong).

https://doi.org/10.1016/j.bioorg.2021.104795
Received 30 December 2020; Received in revised form 22 February 2021; Accepted 2 March 2021
Available online 4 March 2021
0045-2068/

respectively. Certain classes of microtubule modulators have emerged as clinically effective drugs, *e.g.*, *Vinca* alkaloids (destabilising agents) and taxanes (stabilising agents) [1,2]. Despite clinical approval, the adverse effects of these agents are apparent: taxanes are associated with several severe side effects that include neurotoxicity [3], reduced blood cell counts [3,4], muscle and joint pain [5], and cardiotoxicity [6], whereas the *Vinca* alkaloids are associated with neurotoxicity [7,8], hepatotoxicity [9], decreased white blood cell count [10], and hypertension [11]. Thus, novel microtubule modulators with fewer side effects are highly desirable. An additional limitation of these agents is their large molecular size making them difficult to be absorbed through oral administration. Consequently, the drugs are typically administered by intravenous injection, thereby making it inconvenient for patients. To address this limitation, decrease in molecular size with drug-like physicochemical properties are typical traits of orally available drugs. However, despite tremendous developments of small molecular weight tubulin inhibitors, clinical approval has yet to be achieved to treat cancer patients primarily due to lack of effectiveness, pharmacokinetic barriers and selectivity. Most small molecules, which target tubulin inhibit, inhibit the colchicine site, thereby destabilising the microtubule structure. There are numerous drug candidates, which inhibit the colchicine site, having diverse chemical scaffolds, *e.g.*, colchicine derivatives [12], combretastatin derivatives [13], phenstatins [14], podophyllotoxins [15], chalcones [16,17], thienopyridines [18], sulfonamides [19,20], as well as an array of nitrogen-containing heterocycles [21–23]. A major issue in developing small molecule tubulin inhibitors is selectivity, as these molecules exhibit narrow therapeutic indexes, often resulting in toxicity to healthy cells [24]. Therefore, orally available novel selective small molecule drugs with improved therapeutic profiles are highly desirable.

Currently, applications of *in silico* tools to drug discovery and development have been pivotal in identifying and developing new bioactive agents. This is due to cost-effectiveness, ease of use and ability to deliver quality results, *e.g.*, discovery of tirofiban [25]. Some of the approaches include structure-based virtual screening and ligand-based similarity. Structure-based virtual screening revolves screening a 3D library of molecules against 3D structures of proteins of interest by molecular docking [26]. Calculations of scores, binding energies, and binding modes determine ligand–protein complex complementarity [26]. Similarity approaches are used to find structurally similar molecules from databases, often using molecular fingerprints to find matches [27]. Its utility is well-known for rapid structure–activity relationship (SAR) expansion of biologically active scaffolds [28,29]. The Cancer Drug (CDRUG) web server was established to predict anticancer activities of chemical collections based on the chemical fingerprints of molecule datasets from the NCI60 Developmental Therapeutics Program (DTP) [30]. Applying CDRUG to a chemical collection can establish structural similarity relationships between the chemical collection and biologically active molecules from the DTP with anti-proliferative activities. Applying CDRUG to a virtual screening campaign can lead to useful prediction of hit candidates, *e.g.*, identification of anticancer natural products from biodiverse sources [31]. In this project, the aim is to use a combination of CDRUG, structure- and similarity-based virtual screening methods to identify new chemical entities predicted to inhibit tubulin polymerisation with potent anticancer activities. The hit candidates can be tested using *in vitro* assays to verify their biological action. The best candidates are followed by preliminary synthetic modifications to further explore the SAR.

2. Results and discussion

2.1. Screening

2.1.1. Identification of potential anticancer candidates using CDRUG

A collection of ~100,000 molecular entities was used as the input query and filtered using CDRUG to identify potential candidates with anticancer activities. Twenty molecules were selected (Fig. 1) based on colour codes and CDRUG scores that indicate medium to high possibility of anticancer activities (Table S1). Additionally, included in Table S1, are matched chemical structures from the NCI60 DTP database, and NCI60 growth inhibition activities. The selected molecules include moieties with di- and trimethoxy-substituted phenyl rings for **1**, **2**, **5**, **8**, **11** and **15**. Additionally, **11** contains a pyridine. Other nitrogen-containing aromatic heterocycles include tetrazoles for **3**, piperidine for **4**, quinolines for **6** and **13**, pyrimidines for **10**, **12** and **14**, and indoles for **16**–**20**. Molecules **4**, **7**, **9** and **10** are benzodioxole, dibenzazepine, pyridazinone and dihydronaphthalene derivatives, respectively.

2.1.2. Identification of 3-phenyl-1H-indoles as active anticancer scaffolds

To verify their anticancer activities, molecules were tested experimentally against four human cancer cell lines: lung adenocarcinoma (A549), hepatocellular carcinoma (HepG2), cholangiocarcinoma (HuCCA-1), and leukaemia (MOLT-3). The results shown in Table 1 indicate that the MOLT-3 cell line was the most sensitive cell line whereas HepG2 and HuCCA-1 were weakly sensitive, and A549 was insensitive ($IC_{50} > 50$ μM). Molecule **19** exhibited the strongest anticancer activities seen in all four cell lines ($IC_{50} < 33$ μM). Molecule **12** was second best demonstrating activities in three cell lines, MOLT-3, HepG2 and HuCCA-1 ($IC_{50} < 50$ μM). Molecule **20** was third best, displaying $IC_{50} \sim 22$ μM for two cell lines: MOLT-3 and HepG2. Molecules **1**, **7**, **10**, **11** and **18** showed minimal activities, and were only active against MOLT-3 ($IC_{50} < 30$ μM). Interestingly, **19** matched with a 3-phenyl-1*H*-indole, NSC131408365, an anticancer molecule that exhibited strong growth inhibition with $\log GI_{50} = -6.58$ (see Table S1). The 3-phenyl-1*H*-indoles have been established as tubulin inhibitors with anti-proliferative effects [32,33]. Furthermore, five out of the twenty molecules predicted using CDRUG contain 1*H*-indole with three molecules, **16**, **18** and **19**, matching with NSC131408365. These findings encouraged us to further explore the SAR based on the chemical scaffold of **19** to find new inhibitors with improved potencies.

2.1.3. 3-phenyl-1H-indole-2-carbohydrazides as potent anticancer agents

Similarity-based approach was applied using the chemical scaffold of **19** as the search query in the Chembridge online store website. A similarity coefficient value of 0.7 was used, since 0.7 is regarded as being appropriate to expand the SAR of the series, *i.e.*, search outputs result in molecules that are not too structurally similar or different [28]. Two hundred and forty-seven molecules resulted and were downloaded in 3D format, and energy minimised to prepare for virtual screening by molecular docking.

The docking protocol was first validated. The co-crystallised colchicine was removed, energy minimised, and re-docked back to the colchicine site to observe for the reproducibility of the binding orientation of colchicine (see experimental section). The root mean squared deviations (RMSDs) including only heavy atoms were measured for the co-crystallised colchicine and the highest scoring conformation for each scoring function. The RMSD values were calculated: RMSD = 0.53, 0.49, 0.31 and 0.31 Å for scoring functions GoldScore (GS) [34], Chemscore (CS) [35], ChemPLP [36] and Astex Statistical Potential (ASP) [37], respectively. Low RMSD values confirmed comparable binding orientations between the re-docked colchicine and the co-crystallised colchicine.

The molecules were subjected to molecular docking to the colchicine site of tubulin in a virtual screening campaign to predict the best candidates for tubulin inhibition (scores are shown in Table S2). The filter criteria used were GS > 65, CS > 30, ChemPLP > 70 and ASP > 26. A total of twenty-seven molecules resulted. Benzylidene-3-phenyl-1*H*-indole-2-carbohydrazide derivatives were removed as these were reported structures [32,33]. A reported tubulin inhibitor, (*E*)-5-chloro-*N*'-(4-methoxybenzylidene)-3-phenyl-1*H*-indole-2-carbohydrazide (**21a**) [33], that belongs to the benzylidene-3-phenyl-1*H*-indole-2-carbohydrazide class was purchased from InterBioScreen (IBS) to be used as

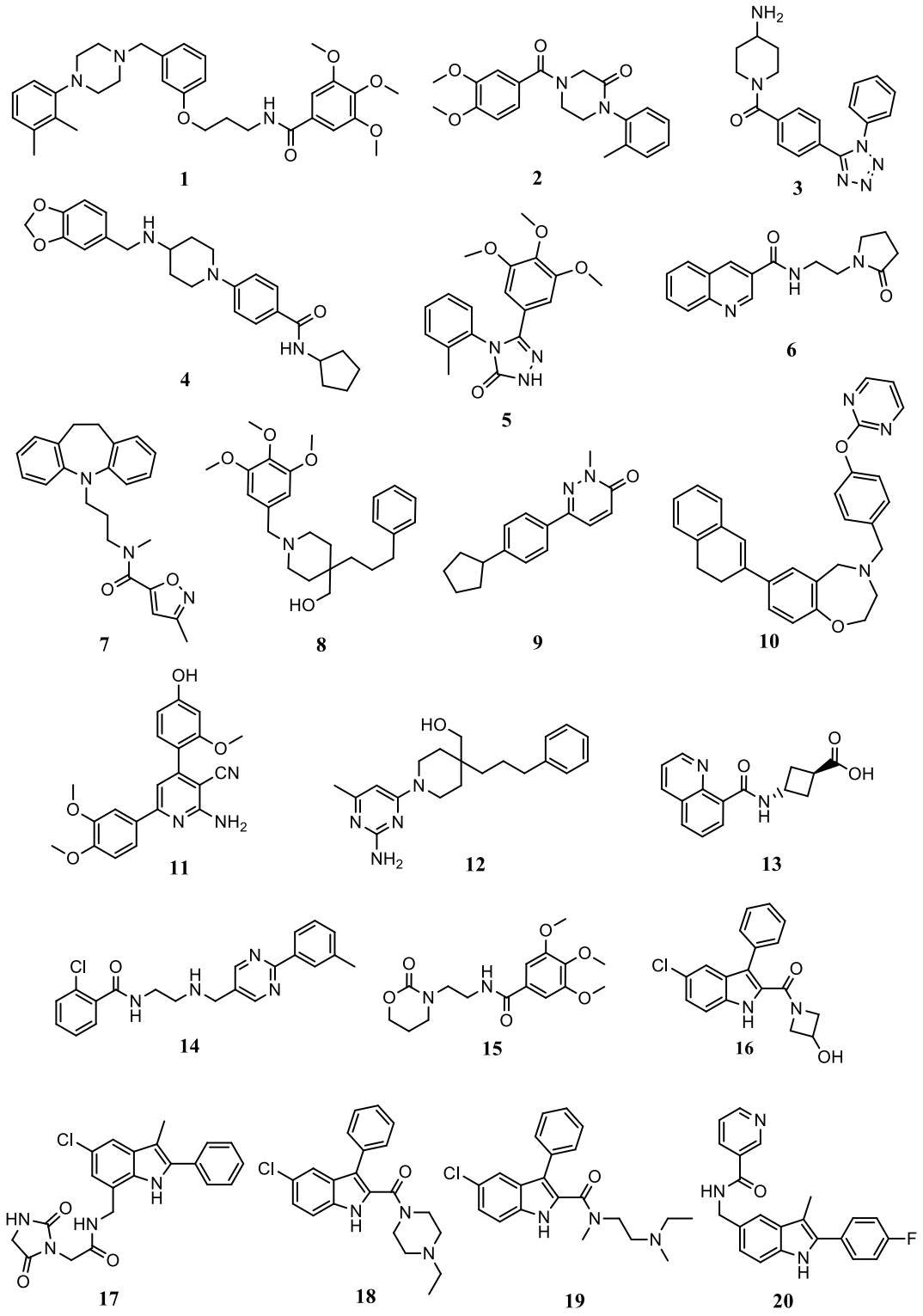

Fig. 1. The chemical structures purchased from Chembridge based on screening using the CDRUG web server.

future experimental control. Three 3-phenyl-1*H*-indole-2-carbohydrazides were obtained from Chembridge: **21b** and **21c** with 1-phenylethylidene, and **22** has a novel *N*-cyclopentylidene of hydrazide (structures in Table 2). All three molecules contain the carbohydrazide functionality, which was presumed to be important for strong antiproliferative activities [32,33,38–40]. Furthermore, the 3-phenyl-1*H*-indole-2-carboxamide molecular scaffold was used as the query for a substructure in the IBS database. Five more 3-phenyl-1*H*-indole-2-carbohydrazides, **23-27a** were identified and purchased from IBS for further experimental testing (structures in Table 2). Molecules **23**, **24** and **25** have cyclohexylidene, hydrogen and acetyl groups substituted at the R_2 position, respectively. Molecules **26** and **27a** are heterocyclic derivatives and contain unsubstituted thiophenyl and furyl moieties, respectively.

Table 1
Selected molecular structures predicted from the CDRUG web server and their anticancer effects in four cancer cell lines: HuCCA-1, A549, MOLT-3 and HepG2. The assay was conducted as three independent experiments and the mean IC_{50} values are shown.

Molecule	HuCCA-1 (μM)	A549 (μM)	MOLT-3 (μM)	HepG2 (μM)
1	>50	>50	16.6 ± 1.4	>50
2	>50	>50	>50	>50
3	>50	>50	>50	>50
4	>50	>50	>50	>50
5	>50	>50	>50	>50
6	>50	>50	>50	>50
7	>50	>50	25.5 ± 0.9	>50
8	>50	>50	>50	>50
9	>50	>50	>50	>50
10	>50	>50	20.2 ± 1.1	>50
11	>50	>50	13.6 ± 0.3	>50
12	43.6	>50	24.3 ± 0.5	16.5 ± 1.1
13	>50	>50	>50	>50
14	>50	>50	>50	>50
15	>50	>50	>50	>50
16	>50	>50	>50	>50
17	>50	>50	>50	>50
18	>50	>50	29.3 ± 0.3	>50
19	32.4 ± 8.9	26.5 ± 1.4	12.7 ± 0.5	15.4 ± 0.6
20	>50	>50	23.1 ± 0.7	20.8 ± 0.8
Doxorubicin[a]	0.92 ± 0.03	0.44 ± 0.10	0.009 ± 0.002	0.57 ± 0.04

[a] Positive control.

2.1.4. Tubulin polymerisation inhibition

The eight 3-phenyl-1*H*-indole-2-carbohydrazides purchased from Chembridge and IBS were further evaluated for tubulin polymerisation inhibition (see Fig. 2A). The molecules showed tubulin inhibition activities but were not as potent compared to the known inhibitor, **21a**. Among the eight molecules, furan-3-ylmethylene-3-phenyl-1*H*-indole-2-carbohydrazide (**27a**) was clearly the best inhibitor with RFU ~ −200 arbitrary units. Molecules **21c** and **21b** were second and third best candidates with RFU ~ 400 and 500 arbitrary units, respectively. Molecules **22**, **23**, and **26** lacked anti-tubulin activities with RFU ~ 600. From the data, **24** and **25** slightly promoted tubulin assembly (RFU ~ 600 to 700). However, this finding seemed doubtful as indole-based molecules have been suggested to inhibit the colchicine site that accommodates small molecules in favour of stabilising site, *e.g.*, taxane. The taxane site is by far more spacious making it suitable to accommodate larger molecules suggesting the colchicine site as a more plausible inhibition site.

The results from this assay prompted us to synthesise derivatives to explore the SAR based on the chemical scaffold of **27a**. Two positions on the scaffold were explored: halogen substitutions at R_1, and halogens and methoxy substitution at R_2 positions. Incorporation of fluorine groups have been suggested to enhance pharmacokinetic properties such as membrane penetration and metabolic stability. This encouraged us to explore fluorine groups at R_1 position. Furthermore, derivatives with halogen and methoxy substitutions at R_2 position (**27b–27h**) and derivatives with 2- (**27i**) and 3-furanyl (**27j**) were synthesised. The

Table 2
Anti-proliferative activities of 3-phenyl-1*H*-indole-carbohydrazides. The assay was conducted as three independent experiments and the mean IC_{50} values are shown.

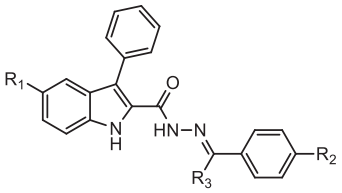

21a-21c

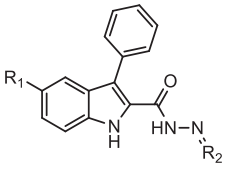

22 - 23

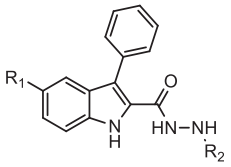

24 - 25

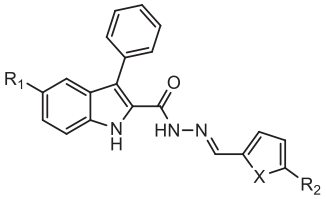

26 - 27h

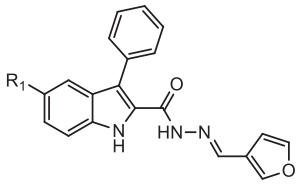

27i - 27j

Molecule	R_1	R_2	R_3	X	HuCCA-1 (μM)	A549 (μM)	MOLT-3 (μM)	HepG2 (μM)
21a[a]	Cl	OCH_3	H	–	>50	>50	0.10 ± 0.02	0.82 ± 0.20
21b	Br	CH_2CH_3	CH_3	–	>50	23.6 ± 2.8	0.87 ± 0.13	3.6 ± 0.4
21c	Cl	CH_2CH_3	CH_3	–	8.3 ± 1.2	6.7 ± 0.4	0.60 ± 0.02	2.3 ± 0.3
22	Cl	*c*-C_5H_8	–	–	>50	>50	10.1 ± 2.4	>50
23	Cl	*c*-C_6H_{10}	–	–	>50	>50	39.0 ± 5.0	>50
24	Cl	H	–	–	>50	>50	9.3 ± 0.9	31.5 ± 0.1
25	Br	$COCH_3$	–	–	>50	>50	35.2 ± 6.4	>50
26	Br	–	–	S	3.6 ± 0.1	0.19 ± 0.01	0.07 ± 0.02	0.73 ± 0.09
27a	Br	–	–	O	33.6 ± 1.2	23.8 ± 3.9	0.47 ± 0.05	1.1 ± 0.3
27b	Br	OCH_3	–	O	0.06 ± 0.01	47.4 ± 0.9	0.09 ± 0.01	0.34 ± 0.01
27c	Br	Cl	–	O	0.46 ± 0.04	14.9 ± 2.2	0.23 ± 0.05	1.6 ± 0.1
27d	Br	Br	–	O	0.38 ± 0.03	0.43 ± 0.09	0.32 ± 0.02	1.7 ± 0.1
27e	F	H	–	O	13.6 ± 2.6	16.2 ± 1.4	0.25 ± 0.06	13.8 ± 2.3
27f	F	OCH_3	–	O	15.5 ± 1.1	20.6 ± 1.9	0.03 ± 0.01	2.0 ± 0.2
27g	F	Cl	–	O	1.6 ± 0.1	18.6 ± 0.1	0.15 ± 0.01	1.8 ± 0.1
27h	F	Br	–	O	1.3 ± 0.2	13.8 ± 0.6	0.17 ± 0.01	3.5 ± 1.7
27i	Br	–	–	–	13.0 ± 0.4	25.7 ± 0.5	0.33 ± 0.05	9.3 ± 1.3
27j	F	–	–	–	1.6 ± 0.1	21.3 ± 0.8	0.51 ± 0.13	10.6 ± 3.5
Doxorubicin[b]	–	–	–	–	1.2 ± 0.4	0.72 ± 0.03	0.024 ± 0.006	0.49 ± 0.02

[a] Reported tubulin inhibitor from Ref. [33].
[b] Positive control.

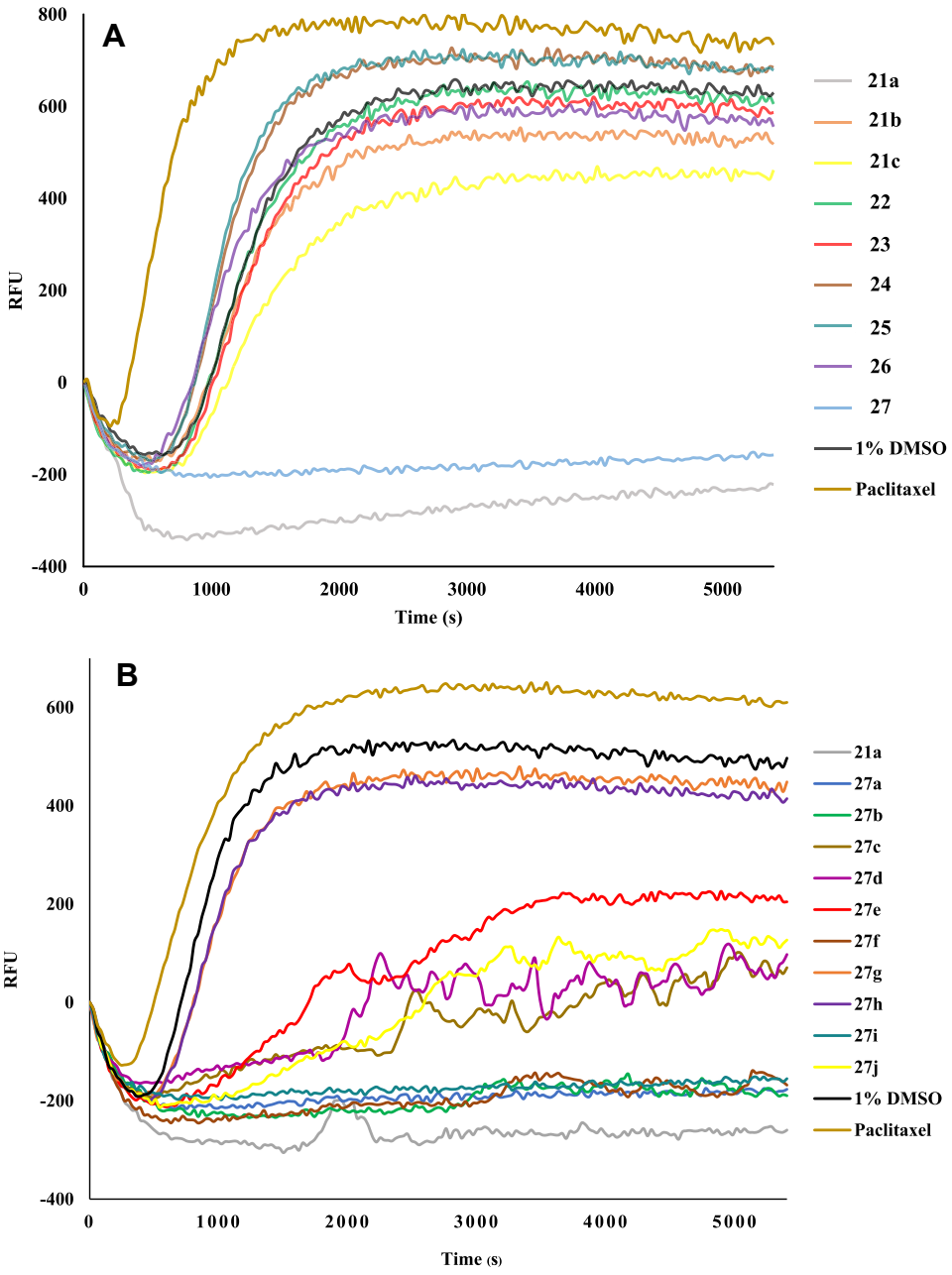

Fig. 2. Effect of 3-phenyl-1*H*-indole-2-carbohydrazide derivatives at 10 μM on tubulin polymerisation at 37 °C with molecule **21a** as the known inhibitor and 10 μM of paclitaxel as the known microtubule-stabilising agent. (**A**) Effect of tubulin polymerisation by molecules **21b**, **21c** and **22-27a**. The curve is the average from two experimental runs (**B**) Tubulin polymerisation inhibition activities of furan-3-ylmethylene-3-phenyl-1*H*-indole-2-carbohydrazide derivatives **27b-27j**. The curves are the averages of three experimental runs.

control molecule, **21a** remained the most potent with RFU ~ −300 arbitrary units. Molecules with bromine at R_1 exhibited strong tubulin inhibition (**27a**, **27b** and **27i**) with RFU ~ −200 arbitrary units, whilst dual halogen substitutions at R_1 and R_2 demonstrated partial tubulin inhibition with RFU ~ 50 to 200 arbitrary units (**27c** and **27d**). Unfortunately, most derivatives with fluorine substitution at R_1 were less potent (**27e**, **27g**, **27h**, and **27j**) than other brominated derivatives. Nevertheless, an exception was seen for **27f** that demonstrated comparable tubulin inhibition to **27a**, **27b** and **27i**. This was evident that methoxy at R_2 position can enhance tubulin inhibition independent of R_1 substitutions. Altering from 2-furyl to 3-furyl position was tolerable as seen for molecules **27a** *vs.* **27i**, and **27e** *vs.* **27j**.

2.1.5. *Biological evaluation of 3-phenyl-1H-indole-2-carbohydrazides*

The 3-phenyl-1*H*-indole-2-carbohydrazides were further subjected to biological evaluation against four cancer cell lines: HuCCA-1, A459, MOLT-3 and HepG2 (Table 2). Analysis of the data in Table 2 suggested the derivatives displayed anti-proliferative properties. The MOLT-3 cell line was the most sensitive followed by HepG2, HuCCA-1 and A459, respectively. Generally, furyl derivatives with bromine at R_1 with halo- and methoxy substitutions at R_2 (**27b-27d**) seemed to demonstrate strongest anti-proliferative effects, *i.e.*, $IC_{50} < 0.5$ μM in HuCCA-1 and MOLT-3 cell lines, and $IC_{50} < 2$ μM for HepG2. Notably, **27b-27d** displayed stronger anticancer effects against the HuCCA-1 cell line than parent molecule, **27a**, and the clinically approved doxorubicin ($IC_{50} <$ 0.5 μM). In particular, **27d** with dual bromine substitutions at R_1 and R_2 also showed improved anti-proliferative activity against the A549 cell line with $IC_{50} = 0.43$ μM compared to doxorubicin ($IC_{50} = 0.72$ μM). In general, the derivatives with fluorine substitutions at R_1 were weaker than their bromo-substituted counterparts, which was apparent in all four cell lines. The results correlate relatively well with tubulin polymerisation inhibition, suggesting tubulin inhibition as the key mechanism of action, *i.e.*, bromo-substituted derivatives tended to display stronger anticancer and anti-tubulin effects than fluoro-substituted derivatives. The 3-furyl derivative seen for **27i** did not significantly increase activity when compared to **27a** for A549 and MOLT-3, whilst

reducing activities by ~ 9 folds against HepG2, and ~ 3 folds against HuCCA-1. Fluoro-substituted derivative **27j** displayed comparable anticancer activities to its bromo-substituted counterpart, **27i**, for A549, MOLT-3 and HepG2 but was ~ 8 fold stronger against the HuCCA-1 cell line.

Cycloalkyl derivatives **22** and **23**, non-substituted **24**, and **25** acetyl substitutions displayed detrimental anti-proliferative activities, *i.e.*, IC_{50} > 50 μM in two to three cell lines: HuCCA-1, A549 and HepG2. Molecule **26** with a thiophenyl moiety displayed the strongest anti-proliferative effects against A549 with IC_{50} = 0.19 μM which was ~3 fold more potent than doxorubicin, and was second best against HepG2 with IC_{50} = 0.73 μM. Regardless, **26** showed poor tubulin inhibitory effect implying a different mode of action that needs further investigation. Molecules **21b** and **21c** with 1-phenylethylidene moieties, showed respectable anti-proliferative effects particularly against MOLT-3 (IC_{50} < 1 μM) and HepG2 (IC_{50} < 4 μM). However, the tubulin polymerisation assay results cannot fully verify the key mechanisms of action of **21b** and **21c**.

We further compared the anticancer activities of unsubstituted furyl- (**27a**) and thiophenyl- (**26**) 3-phenyl-1*H*-indole-2-carbohydrazide series to the predecessor benzylidene-3-phenyl-1*H*-indole-2-carbohydrazides; the known tubulin inhibitor **21a** showed adequate anti-proliferative activities against MOLT-3 (IC_{50} = 0.87 μM) and HepG2 (IC_{50} = 3.6 μM) and detrimental activities against HuCCA-1 and A549 (IC_{50} > 50 μM), and ten additional benzylidene-3-phenyl-1*H*-indole-2-carbohydrazide derivatives (**21d–21m**) which were purchased from IBS and tested experimentally against the same four cancer cell lines (Table S3). From the data, it was clear that the furyl- and thiophenyl-3-phenyl-1*H*-indole-2-carbohydrazide series demonstrated stronger anti-proliferative activities than the predecessed benzylidene-3-phenyl-1*H*-indole-2-carbohydrazides.

2.2. Cell cycle analysis

Abolishment of microtubule function and arrest in the at G2/M phase of cell cycle by tubulin inhibitors are well-documented [41]. Therefore, the three molecules, **21c**, **26**, and **27a**, with differential effects on tubulin polymerisation were selected for further study on cell cycle progression. After treatment with the three molecules at 10 μM concentration for 16 hrs on A549 lung cancer cells, spherical cell shapes were observed (Fig. 3A) concomitant with increasing proportion of cells in G2/M phase (Fig. 3B and C), indicating all the three molecules were able to induce cell cycle arrest at the G2/M phase. Treatment with **27a**, a pre-established potent inhibitor of tubulin polymerisation, and **21c**, a mild inhibitor, elevated the proportion of cells in the G2/M phase by 81.1 ± 2.4% and 79.1 ± 8.6%, respectively, compared with 33.4 ± 2.0% in vehicle-treated cells (Fig. 3C). Interestingly, **26** which possessed strong anti-proliferative effects but did not inhibit tubulin polymerisation also increased the number of cells in the G2/M phase by 57.8 ± 4.3% (Fig. 3C). The results suggested that molecules **21c** and **26** induced G2/M cell cycle arrest by mechanisms other than the tubulin inhibition. Several reports have shown that the arrest of G2/M phase in A549 cells could be achieved by inhibition of targeted proteins other than tubulin, *e.g.*, topoisomerase II [42], aurora kinase-B [43], and DNA methyltransferase [44]. The mechanisms underlying the G2/M phase arrest by **21c** and **26** are to be investigated further.

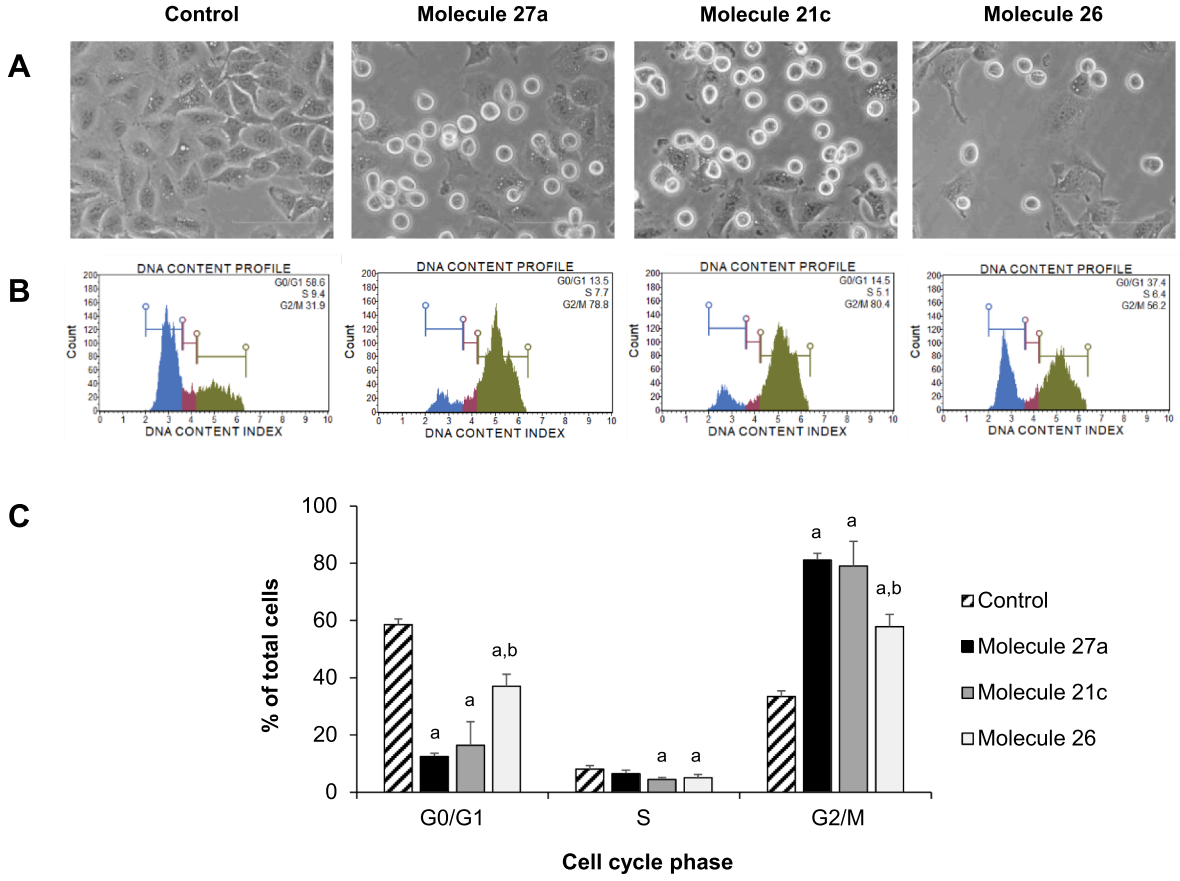

Fig. 3. Effect of molecule **27a**, **21c**, and **26** on cell cycle phase distribution of A549 lung cancer cells. The cells were treated with vehicle or 10 μM of each compound for 16 hrs. The percentages of cells in G0/G1, S, and G2/M phases were analyzed by using Muse Cell Analyzer with Muse Cell Cycle Assay kit. (**A**) Representative images of cell morphology after treatment (×200 magnification). (**B**) Histograms of DNA content in treated cells from a representative experiment. (**C**) The percentages of cells in G0/G1, S, and G2/M phases after treatment. Data are expressed as average with SD from three independent experiments. a, significant difference from control ($p < 0.05$); b, significant difference from molecule **27a** and **21c** ($p < 0.05$).

2.3. Synthesis of furan-3-ylmethylene-3-phenyl-1H-indole-2-carbohydrazides

The synthesis of the derivatives **27a-27j** is described in Scheme 1. Ethyl acetoacetate **28** was used as the starting material to prepare ketobutanoate **29** by alkylation with benzylbromide. By applying the Japp-Klingemann reaction [45–48], ketobutanoate **29** was treated with *p*-bromo- and chloro-benzene diazonium salts **30a** and **30b** to give intermediate **31**. Without further purification, **31** was subjected to Fischer indole synthesis [49,50] to afford indole **32** with high yields for both bromo- and chloro-derivatives. The carbohydrazine functionality of intermediate **33** was formed by the treatment of indole **32** with hydrazine. Condensations of hydrazine with various substituted furfurals obtained derivatives **27a-27j** as the final products; the yields are shown in Table S4. It should be noted that hydrazine condensation with aldehydes was expected to give *E*- and *Z*-isomeric mixtures, but only the more chemically stable *E*-isomer products were isolated [51–53].

2.4. Molecular modelling

2.4.1. Molecular docking analysis

To gain further insight into the mode of binding of the furan-3-ylmethylene-3-phenyl-1*H*-indole-2-carbohydrazides, the molecules were docked to the colchicine binding site of tubulin located at the interface between α- and β- subunits. The scores are shown in Table S2. The predicted binding orientations of the series were more or less similar, and can be represented by molecules **27a** and **27b** shown in Fig. 4. Hydrophobic indole and 3-phenyl groups occupied the hydrophobic pockets of the β-subunit. This was seen to be favourable as indole is well-known for its role in tubulin inhibition [21], and 3-methyl substitution on the indole scaffold have been reported to lower anticancer activities [33] suggesting decreased binding affinity probably as a result of decreased hydrophobic contacts. Hydrophobic interactions were formed between the inhibitors and hydrophobic residues, *e.g.*, Val181, Ala180 and Leu255. Additionally, observations of hydrophobic contacts to Lys254, Asn258, Asn349, Lys352 and Thr179 were seen with non-polar parts of the residue structures. The hydrazide arm linked to furan orientate towards α-tubulin. Hydrogen bonding interactions were predicted between indole and Thr179, and occasionally between furan and residue side chains of Ser178 and Lys243. The methylene and furan ring were predicted to form hydrophobic contacts with Leu248, Tyr224, Gln11, Gln247, Asn249, and Lys254. The amino acid residues mentioned have been reported to contribute to tubulin inhibition by the theinopyridine [18], indolizine [54], and cyclohexanedione [55] derivatives.

2.4.2. Chemical space

On grounds that the 3-phenyl-1*H*-indole-2-carbohydrazides were investigated to be developed as anticancer agents, their physicochemical properties were evaluated against benchmarks such as the Lipinski's filters [56] and Veber's rule [57] established to assess the drug-like properties. The molecular descriptors are molecular weight, hydrogen bond donor and acceptor, rotatable bond, topological polar surface area, and lastly, Moriguchi log P (*M*logP) [58] that calculates lipophilicity. The calculated molecular descriptors are shown in Table S5 revealing the derivatives to be within the drug-like chemical space, *i.e.*, the numerical figures did not exceed the Lipinski's or Veber's limit. This determined the derivatives as pharmacokinetically favourable scaffolds for drug development.

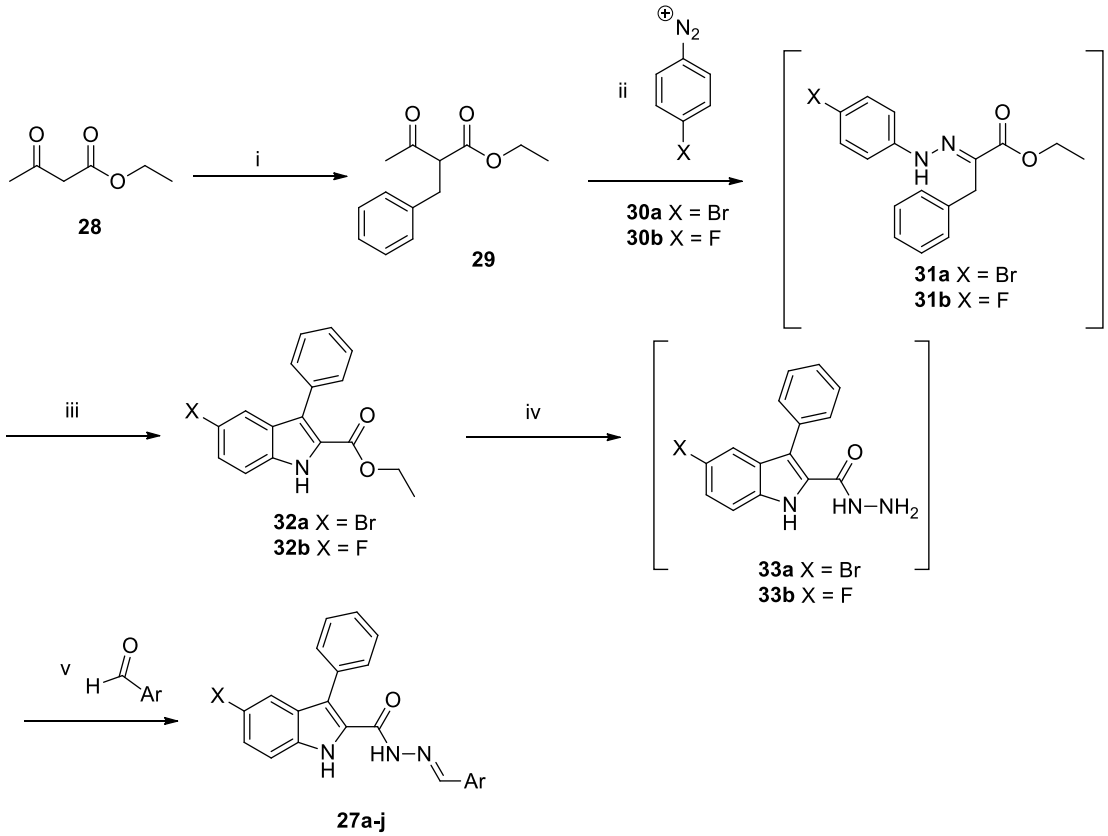

Scheme 1. Synthesis of furan-3-ylmethylene-3-phenyl-1*H*-indole-2-carbohydrazide derivatives reagents and conditions: (i) NaH, THF, 0-5 °C, 10 min, rt, BnBr then reflux 17 hrs, 64%; (ii) KOH, EtOH, H_2O, **30a** or **30b**, 0 °C, 10 min then refrigerated 17 hrs; (iii) HCl, 80 °C, 4 hrs, **32a** 88% **32b** 79%; (iv) N_2H_4, EtOH, 80 °C, 17 hrs; (v) ArCHO, EtOH, 80 °C, 3 hrs.

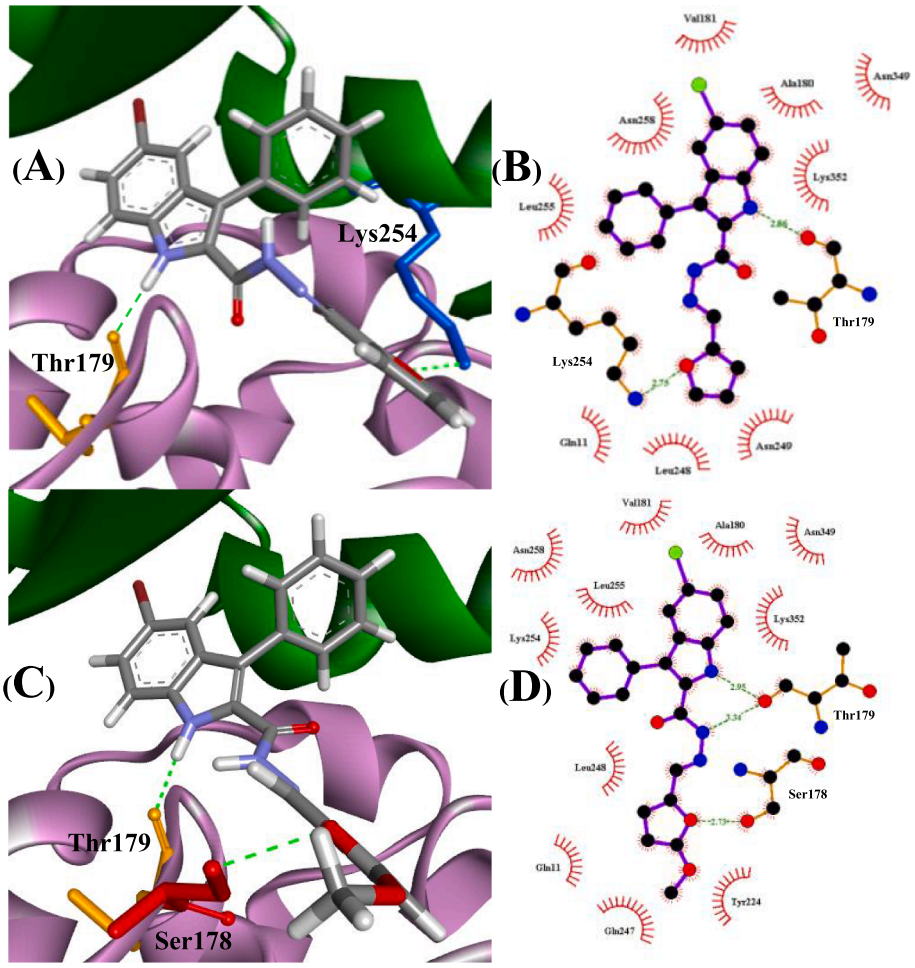

Fig. 4. The binding modes and interactions of furan-3-ylmethylene-3-phenyl-1*H*-indole-2-carbohydrazides to the colchicine site of tubulin using molecular docking based on the top scoring conformation from GoldScore. The hydrogen bonds are represented as green dotted lines. Binding mode depictions of molecules **27a** (**A**) and **27b** (**C**) to the colchicine site. Green ribbons represent β-tubulin whereas pink ribbons represent α-tubulin. Hydrogen bonding residues Thr179, Lys254 and Ser178 are shown in orange, blue and red sticks, respectively. Two-dimensional illustrations of intermolecular interactions between tubulin, and molecules **27a** (**B**) and **27b** (**D**). The hydrophobic interactions are represented as red lashes. Hydrogen bond distances in angstrom units are shown.

3. Conclusion

In this study, a combination of *in silico* screening, *in vitro* testing and synthesis have led to the identification of new biologically active derivatives of 3-phenyl-1*H*-indole-2-carbohydrazides with anti-proliferative properties: furan-3-ylmethylene-3-phenyl-1*H*-indole-2-carbohydrazides (**27a-27j**) that inhibit tubulin polymerisation, a highly potent thiophenyl derivative **26**, and phenylethylidene derivatives **21b** and **21c**. Tubulin polymerisation assay results revealed derivatives with bromine were more favourable than fluorine substitutions at C5. Furthermore, methoxy substitutions on the furan ring showed prominent anti-tubulin activities, whereas change from 3- to 2-furyl was tolerable. The study was unable to clarify the key mechanisms of action of thiophenyl **26** and phenylethylidene **21c** although they clearly demonstrated potent anti-proliferative properties and G2/M phase arrest in A549 cell line. Thus, further investigation into their mechanisms of action is needed. The phenylethylidene, furyl and thiophenyl derivatives showed improved and competent anticancer effects in comparison to the predecessed benzylidene-3-phenyl-1*H*-indole-2-carbohydrazides. Additionally, thiophenyl **26**, and furyl **27b-27d** derivatives were more potent than the clinically approved doxorubicin drug in some cell lines. Molecular docking predicted inhibition of the colchicine site by furyl derivatives **27a-27j**, and formed hydrogen bonding and hydrophobic interactions with important amino acid residues that contribute to perturbation of microtubule dynamics. Furthermore, the calculated physicochemical properties showed that the derivatives are pharmacokinetically favourable scaffolds for drug development.

4. Experimental section

4.1. *In silico screening*

4.1.1. *Ligand preparation*

A commercially available library of ~100,000 small molecules was downloaded from ChemBridge Corporation website in 3D format. The company is a leading global provider of small molecule drug discovery with a portfolio that includes >1.3 million diverse compounds. The quality and reliability of their products adhere to collaborations with leading global pharmaceutical companies. The Scigress software version 2.8.1 was used to remove any counter ions and salts. Hydrogen atoms were added to the molecules followed by energy minimisation using the MM2 [59] force field.

4.1.2. *Screening for candidates with anticancer properties using CDRUG*

The CDRUG webserver can be used as an online tool to predict for the anticancer activity of molecular structures. An active dataset of 8565 anticancer compounds and an inactive dataset consisting of 9804 compounds from the NCI60 Developmental Therapeutics Program (DTP) project were used for benchmarking purposes. Molecular fingerprints and Tanimoto similarity methods were incorporated to identify molecules with potential anticancer properties, in which a final score is calculated as a quantitative measurement.

4.1.3. *Structure-based virtual screening*

Ligands were docked to the crystal structure of tubulin (PDB ID: 4O2B, resolution 2.3 Å) which was obtained from the Protein Data Bank (PDB) [60]. The co-crystallised colchicine ligand and spectator ligands

including crystallographic waters were removed. The centre of the binding pocket was defined at coordinates (x = 13.222, y = 8.371, z = –23.331) with 10 Å radius. Fifty docking runs were allowed for each ligand with default search efficiency (100%). The basic amino acids, lysine and arginine, were defined as protonated and acidic residues, aspartic and glutamic acids were deprotonated. The Goldscore (GS), ChemScore (CS), ChemPLP and Astex Statistical Potential (ASP) scoring functions were implemented to validate the predicted binding modes and relative energies of the ligands using the GOLD version 5.8.1 software suite. Three-dimensional illustrative depictions of binding modes were constructed using Discovery Studio, and two-dimensional diagram plots depicting intermolecular interactions were constructed using LigPlot [61].

4.2. In vitro screening

4.2.1. Anti-proliferative assay

The cell lines used in this study were either purchased from the American Type Culture Collection (ATCC, Manassas, VA, USA) or received as gifts from other sources. Dulbecco's Modified Eagle Medium (DMEM), as well as Ham's F12 and RPMI 1640 media, were supplied in powder form by HyClone Laboratories (Logan, UT, USA), while fetal bovine serum (FBS) and 0.25% trypsin-EDTA were obtained from J R Scientific, Inc. (Woodland, CA, USA) and Gibco (Grand Island, NY, USA), respectively. In addition, bovine insulin, DMSO, doxorubicin, etoposide, glucose, l-glutamine, MTT (3-(4,5-dimethylthiazol-2-yl)-2,5-diphenyltetrazoliumbromide), penicillin–streptomycin, phenazine methosulfate (PMS), and sodium pyruvate were supplied by Sigma–Aldrich (St. Louis, MO, USA), whereas XTT (2,3-bis-(2-methoxy-4-nitro-5-sulfophenyl)-2*H*-tetrazolium-5-carboxanilide) was from Fluka Chemie (St. Louis, MO, USA).

HuCCA-1, A549 and HepG2 cell lines were adherent to the culture wells, whereas only MOLT-3 was grown in suspension. Each cell line was maintained in an appropriate culture medium supplemented with essential nutrients and maintained using standard procedures at 37 °C with 95% humidity and 5% CO_2. All the test molecules and doxorubicin were prepared as 10 mg/mL stock solutions in DMSO and freshly diluted with the corresponding cell culture medium for each cell line on the day of analysis.

Prior to the assay, the cells were inoculated as a suspension in the corresponding cell culture medium (100 μL for adherent cells and 75 μL for suspended cells) into 96-well microtiter plates (Costar No. 3599, Corning Incorporated, Corning, NY, USA) at a density of 5000–20,000 cells per well, depending on their growth rates. Adherent and suspended cells were then allowed to grow at 37 °C with 95% humidity and 5% CO_2 for 24 hrs and 30 min, respectively. The cytotoxicity assay was initiated by adding an equal volume of cell culture medium containing either each test compound, positive control, or DMSO, at predetermined concentrations. Following 48 hrs of exposure to various treatments, cell viability was determined using MTT assay for adherent cells or XTT assay for suspended cells, as described below.

For adherent cells, 100 μL of the MTT reagent (0.5 mg/mL in serum-free cell culture medium) was added to each well, and the microtiter plates were further incubated for 2.5–4 hrs at 37 °C with 95% humidity and 5% CO_2. The medium was subsequently replaced with 100 μL of DMSO to dissolve the purple formazan before the absorbance at 550 nm was measured using a Spectra-Max Plus 384 microplate reader (Molecular Devices, Sunnyvale, CA, USA) with a reference wavelength of 650 nm.

For suspended cells, 75 μL of the XTT reagent (prepared from 5 mL of 1 mg/mL XTT sodium in water and 100 mL of 0.383 mg/mL PMS in water) was added to each well, and the cells were further incubated for 4 hrs at 37 °C with 95% humidity and 5% CO_2. Afterwards, the absorbance of orange formazan at 492 nm was measured with a reference wavelength of 690 nm using a SpectraMax Plus 384 microplate reader. For each well, the background absorbance (averaged from the wells containing the same volume of complete culture medium) was subtracted from either A550 or A492 to get the absolute absorbance. The average value from the duplicate wells, which had been treated with each concentration of the test molecules, was then compared with that of the untreated wells to yield the percentage of surviving cells. The IC_{50} value was finally calculated from the dose–response curve as the concentration that inhibits the cell growth by 50% in comparison with the negative control following 48 hrs of exposure to each test molecule.

This assay protocol can be applied for use to test the anti-proliferative activities of anti-tubulin agents as shown in Table S6, nocodazole was tested using the same protocol.

4.2.2. Tubulin polymerization assay

Inhibitory effect of test molecules on tubulin polymerization was analyzed using a commercial fluorescence-based tubulin polymerization assay kit (Cytoskeleton, catalog no. BK011P) according to the manufacturer's protocol. Briefly, 5 μL of test molecules at indicated concentration was mixed with 50 μL of tubulin reaction mixture containing free porcine brain tubulin (2 mg/ml) in buffer supplemented with 20% glycerol and 1 mM GTP on ice. The fluorescence intensity was measured every 30 s for 90 min at 37 °C using a fluorescence microplate reader (BioTek Instruments). The excitation and emission wavelengths were 360 and 450 nm, respectively.

4.3. Cell cycle

Effect of test molecules on cell cycle phase distribution was investigated by flow cytometric technique using Muse Cell Analyzer with the Muse Cell Cycle Assay kit (Luminex, USA). Briefly, A549 cells (1.5×10^5 cells/well) in 6-well plate were treated with test molecules at 10 μM or vehicle (0.2% DMSO) for 16 hrs. After treatment, the cells were harvested by trypsinization and prepared for cell cycle analysis according to the kit's protocol. Results were expressed as percentages of cell populations in G0/G1, S, and G2/M phases.

4.4. Molecular descriptor calculations

The Dragon software package was used to calculate the molecular descriptors of the compounds.

4.5. Synthesis

All chemical reagents and solvents were brought from commercial suppliers and used directly unless specific stated. Thin layer chromatography was performed on Merck silica gel 60 F254 plates and visualized by UV irradiation at 254 nm. Flash column chromatography was performed using Silicycle SilicaFlash® F60 (40–63 μm). ^{1}H NMR spectra were recorded on a Bruker AVANCE-300 MHz. Chemical Shifts (δ) are reported in parts-*per*-million (ppm) with respect to the solvent peaks and coupling constants (*J*) are in Hertz. NMR peak multiplicities are given the abbreviations: s = singlet, d = doublet, t = triplet, q = quartet, m = multiplet, br = broad. ^{13}C NMR spectra were recorded on a Bruker AVANCE-75 MHz. Chemical Shifts (δ) are reported in parts-*per*-million (ppm) with respect to the solvent peaks and coupling constants (*J*) are in Hertz. ^{19}F NMR spectra were recorded on a Bruker AVANCE-282 MHz. Chemical Shifts (δ) are reported in parts-*per*-million (ppm) with respect to the solvent peaks. Infrared (IR) spectra were recorded on Thermo Scientific Nicolet iS 5 Fourier Transform IR spectrometer. Only selected peaks are reported and absorption maxima are given in cm^{-1}. High Resolution mass spectra (HR-MS) were obtained on a Thermo Scientific orbitrap Q Exactive Focus mass spectrometer. Melting points were recorded using a Stuart SMP30 capillary melting point apparatus.

4.5.1. Ethyl 2-benzyl-3-oxobutanoate (**29**)

Under Argon atmosphere, anhydrous THF (20 mL) was added to NaH (60% in oil, 0.69 g, 17.43 mmol), and the mixture was cooled to 0 °C.

With a magnetic stirring, ethyl acetoacetate **28** (2.00 mL, 15.89 mmol) was added dropwise. The mixture was stirred until the gas evolution finished and then warmed to room temperature. Benzyl bromide (2.80 mL, 23.54 mmol) was added dropwise, and the mixture was heated to 72 °C. After 16 hrs, the mixture was allowed to cool to room temperature. The mixture was diluted by saturated aqueous ammonium chloride (10 mL) and was extracted with Et_2O (3 × 20 mL). The combined organic layers were dried (Na_2SO_4), filtered, and solvent was evaporated. Purification by flash column chromatography, eluted with EtOAc-Hexane (0.5:9.5 to 1:9), gave ethyl 2-benzyl-3-oxobutanoate **29** (2.23 g, 10.12 mmol, 64%) as an oil; R_f 0.3 [EtOAc-Hexane (1:9)]; ^{1}H NMR (300 MHz, $CDCl_3$) δ 7.31–7.18 (m, 5H, Ph), 4.17 (q, J = 7.2 Hz, 2H, OCH_2CH_3), 3.80 (t, J = 7.6 Hz, 1H, CH), 3.19 (d, J = 7.6 Hz, 2H, CH_2), 2.20 (s, 3H, CH_3), 1.21 (t, J = 7.2 Hz, 3H, OCH_2CH_3); ^{13}C NMR (75 MHz, $CDCl_3$) δ 202.50 (C═O), 169.14 ($CO_2CH_2CH_3$), 138.17 (C-Ph), 128.81 (2 × CH-Ph), 128.59 (2 × CH-Ph), 126.69 (CH-Ph), 61.48 (OCH_2CH_3), 61.31 (CH), 33.99 (CH_2), 29.63 (CH_3), 14.03 (OCH_2CH_3). The data was consistent with that in the literature [62].

4.5.2. Ethyl 5-bromo-3-phenyl-1H-indole-2-carboxylate (32a)

To a solution of 4-bromoaniline (0.39 g, 2.27 mmol) in EtOH/H_2O (1:1, 2 mL), were added 0.6 mL conc. HCl and a solution of $NaNO_2$ (0.240 g, 3.48 mmol) in H_2O (10 mL) dropwise at 0 °C. The resulting solution of diazonium salt **30a** was poured into a mixture of ethyl 2-benzyl-3-oxobutanoate (**29**) (0.50 g, 2.27 mmol) and KOH (0.61 g, 10.90 mmol) in EtOH/H_2O (1:1, 2 mL) at 0 °C. The resulting mixture was refrigerated at approximately 4 °C for 17 hrs. The resulting mixture was allowed to warm to room temperature, diluted with H_2O (10 mL) and extracted with EtOAc (3 × 20 mL). The combined organic layers were dried (Na_2SO_4), filtered, and solvent was evaporated to give a crude of hydrazone intermediate **31a** as an oil (used without purification). A solution of the hydrazone crude **31a** in conc. HCl (2.3 mL) was heated to 80 °C. After 4 hrs, the mixture was allowed to cool to room temperature. The mixture was diluted by EtOAc (10 mL) and H_2O (10 mL), then extracted with EtOAc (3 × 15 mL). The combined organic layers were dried (Na_2SO_4), filtered, and solvent was evaporated. Purification by flash column chromatography, elute with EtOAc-Hexane (0.5:9.5 to 2:8), gave indole **32a** (0.69 g, 2.00 mmol, 88%) as a yellow solid; R_f 0.4 [EtOAc-Hexane (1:9)]; m.p. 181–183 °C, lit.[63] m.p. for **32a** 174–175 °C; ν_{max}/cm^{-1} 3304, 3057, 2987, 2940, 1677, 1256; ^{1}H NMR (300 MHz, DMSO-d_6) δ 12.14 (s, 1H, NH), 7.56 (br d, J = 1.8 Hz, 1H, H4-ind), 7.49–7.34 (m, 7H, H6-ind, H7-ind, PhH), 4.22 (q, J = 7.1 Hz, 2H, CH_2), 1.15 (t, J = 7.1 Hz, 3H, CH_3); ^{13}C NMR (75 MHz, DMSO-d_6) δ 161.45 (C═O), 135.20 (C7a-ind), 133.34 (C1′-Ph), 130.83 (C2′-Ph), 128.90 (C2-ind), 128.37 (C3′-Ph), 128.18 (C3a-ind), 127.60 (C4′-Ph), 124.48 (C6-ind), 122.97 (C4-ind), 122.18 (C3-ind), 115.34 (C7-ind), 113.48 (C5-ind), 60.98 (CH_2), 14.38 (CH_3); HRMS (ESI) m/z $[M+H]^+$ calcd for $C_{17}H_{15}O_2N^{79}Br$ 344.0281; found 344.0280.

4.5.3. Ethyl 5-Fluoro-3-phenyl-1H-indole-2-carboxylate (32b)

To a solution of 4-fluoroaniline (0.22 mL, 2.32 mmol) in EtOH/H_2O (1:1, 2 mL), were added 0.6 mL conc. HCl and a solution of $NaNO_2$ (0.240 g, 3.48 mmol) in H_2O (10 mL) dropwise at 0 °C. The resulting solution of diazonium salt **30b** was poured into a mixture of ethyl 2-benzyl-3-oxobutanoate (**29**) (0.51 g, 2.32 mmol) and KOH (0.61 g, 10.90 mmol) in EtOH/H_2O (1:1, 2 mL) at 0 °C. The resulting mixture was refrigerated at approximately 4 °C for 17 hrs. The resulting mixture was allowed to warm to room temperature, diluted with H_2O (10 mL) and was extracted with EtOAc (3 × 20 mL). The combined organic layers were dried (Na_2SO_4), filtered, and solvent was evaporated to give a crude intermediate hydrazone **31b** as an oil (used without purification). A solution of the hydrazone crude **31b** in conc. HCl (2.3 mL) was heated to 80 °C. After 4 hrs, the mixture was allowed to cool to room temperature. The mixture was diluted by EtOAc (10 mL) and H_2O (10 mL), then extracted with EtOAc (3 × 15 mL). The combined organic layers were dried (Na_2SO_4), filtered, and solvent was evaporated. Purification by flash column chromatography, elute with EtOAc-Hexane (0.5:9.5 to 2:8), gave indole **32b** (0.51 g, 1.89 mmol, 81%) as a yellow solid; R_f 0.4 [EtOAc-Hexane (1:9)]; m.p. 144–147 °C; ν_{max}/cm^{-1} 3308, 3063, 2991, 2943, 1677, 1248; ^{1}H NMR (300 MHz, DMSO-d_6) δ 12.02 (s, 1H, NH), 7.52–7.30 (m, 6H, ArH), 7.19–7.11 (m, 2H, ArH), 4.20 (q, J = 7.1 Hz, 2H, CH_2), 1.14 (t, J = 7.1 Hz, 3H, CH_3); ^{13}C NMR (75 MHz, DMSO-d_6) δ 161.07 (C═O), 159.20 (d, J = 234.5 Hz, C5-ind), 133.17 (C1′-Ph), 132.90 (C7a-ind), 130.31 (C2′-Ph), 127.86 (C3′-Ph), 127.00 (C4′-Ph), 126.88 (d, J = 9.8 Hz, C3a-ind), 124.42 (C2-ind), 122.34 (d, J = 5.5 Hz, C3-ind), 114.28 (d, J = 10.1 Hz, C7-ind), 113.93 (d, J = 26.3 Hz, C6-ind), 104.69 (d, J = 23.6 Hz, C4-ind), 60.43 (CH_2), 13.92 (CH_3); ^{19}F NMR (282 MHz, DMSO-d_6) δ −122.57; HRMS (ESI) m/z $[M+H]^+$ calcd for $C_{17}H_{15}O_2NF$ 284.1081; found 284.1084.

4.5.4. (E)-5-bromo-N'-(furan-2-ylmethylene)-3-phenyl-1H-indole-2-carbohydrazide (27a)

To a solution of indole **31a** (0.106 g, 0.31 mmol) in EtOH (15 mL) was added hydrazine (50% in H_2O, 0.58 mL, 9.3 mmol) and the reaction mixture was heated to 80 °C. After 16 hrs, the mixture was allowed to cool to room temperature and solvent was evaporated to give a crude intermediate hydrazide **33a** as a solid (used without purification). To a solution of the hydrazide crude **33a** in EtOH (20 mL) was added furfural (0.03 mL, 0.31 mmol) at room temperature, then the mixture was heated to 80 °C. After 4 hrs, the mixture was allowed to cool to room temperature, and solvent was evaporated. Purification by flash column chromatography, eluted with EtOAc-Hexane (1:9 to 2:3), gave hydrazide **27a** (0.099 g, 0.24 mmol, 77%) as a yellow solid; R_f 0.5 [EtOAc-Hexane (4:6)]; m.p. 231–233 °C; ν_{max}/cm^{-1} 3297, 3173, 3053, 2961, 2926, 1636, 1621, 1264; ^{1}H NMR (300 MHz, DMSO-d_6) δ 12.17 (s, 1H, CONH), 11.37 (s, 1H, NH), 7.94 (br s, 1H, H4“-furan), 7.82 (s, 1H, HC = N), 7.72 (d, J = 1.8 Hz, 1H, H4-ind), 7.48–7.37 (m, 7H, H6-ind, H7-ind, PhH), 6.90 (br s, 1H, H2”-furan), 6.60 (br s, 1H, H3“-furan); ^{13}C NMR (75 MHz, DMSO-d_6) δ 158.10 (C═O), 149.10 (C1”-furan), 145.38 (C4“-furan), 137.17 (C═N), 134.36 (C7a-ind), 132.93 (C1′-Ph), 129.57 (C2′-Ph), 128.67 (C2-ind), 128.55 (C3′-Ph), 127.81 (C3a-ind), 126.90 (C4′-Ph), 126.57 (C6-ind), 121.93 (C4-ind), 117.40 (C3-ind), 114.51 (C7-ind), 114.01 (C2”-furan), 112.99 (C5-ind), 112.24 (C3“-furan); HRMS (ESI) m/z $[M+H]^+$ calcd for $C_{20}H_{15}O_2N_3^{79}Br$ 408.0342; found 408.0344. Compounds **27b-27j** were synthesized following the procedure described here.

4.5.5. (E)-5-bromo-N'-((5-methoxyfuran-2-yl)methylene)-3-phenyl-1H-indole-2-carbohydrazide (27b)

Yellow solid (0.078 g, 0.18 mmol, 58%); R_f 0.5 [EtOAc-Hexane (2:3)]; m.p. 215–218 °C decomposed; ν_{max}/cm^{-1} 3286, 3175, 3030, 2934, 2851, 1741, 1622, 1602, 1261; ^{1}H NMR (300 MHz, DMSO-d_6) δ 12.14 (s, 1H, CONH), 11.18 (s, 1H, NH), 7.73–7.71 (m, 2H, HC = N and H4-ind), 7.51–7.32 (m, 7H, H6-ind, H7-ind, PhH), 6.84 (d, J = 3.0 Hz, 1H, H2“-furan), 5.56 (d, J = 3.0 Hz, 1H, H3”-furan), 3.89 (s, 3H, OCH_3); ^{13}C NMR (75 MHz, DMSO-d_6) δ 163.65 (C4“-furan), 158.28 (C═O), 139.69 (C1”-furan), 137.37 (C═N), 134.77 (C7a-ind), 133.43 (C1′-Ph), 130.01 (C2′-Ph), 129.43 (C2-ind), 129.01 (C3′-Ph), 128.32 (C3a-ind), 127.34 (C4′-Ph), 126.90 (C6-ind), 122.32 (C4-ind), 118.47 (C2“-furan), 117.52 (C3-ind), 114.93 (C7-ind), 113.39 (C5-ind), 83.55 (C3”-furan), 58.64 (OCH_3); HRMS (ESI) m/z $[M+H]^+$ calcd for $C_{21}H_{17}O_3N_3^{79}Br^{35}Cl$ 438.0448; found 438.0449.

4.5.6. (E)-5-bromo-N'-((5-chlorofuran-2-yl)methylene)-3-phenyl-1H-indole-2-carbohydrazide (27c)

Yellow solid (0.076 g, 0.17 mmol, 59%); R_f 0.5 [EtOAc-Hexane (2:3)]; m.p. 231–234 °C; ν_{max}/cm^{-1} 3259, 3135, 3052, 2922, 2850, 1741, 1633, 1618, 1248; ^{1}H NMR (300 MHz, DMSO-d_6) δ 12.15 (s, 1H, CONH), 11.43 (s, 1H, NH), 7.84 (s, 1H, HC = N), 7.70 (d, J = 1.8 Hz, 1H, H4-ind), 7.46–7.32 (m, 7H, H6-ind, H7-ind, PhH), 6.96 (br s, 1H, H2“-furan), 6.61 (br s, 1H, H3”-furan); ^{13}C NMR (75 MHz, DMSO-d_6) δ 158.24 (C═O), 148.88 (C1“-furan), 137.62 (C═N), 135.99 (C4”-furan),

134.42 (C7a-ind), 132.85 (C1′-Ph), 129.56 (C2′-Ph), 129.40 (C2-ind), 128.55 (C3′-Ph), 127.81 (C3a-ind), 126.94 (C4′-Ph), 126.64 (C6-ind), 121.95 (C4-ind), 117.58 (C3-ind), 116.52 (C2"-furan), 114.55 (C7-ind), 113.01 (C5-ind), 109.50 (C3"-furan); HRMS (ESI) *m/z* $[M+H]^+$ calcd for $C_{20}H_{14}O_2N_3^{79}Br^{35}Cl$ 441.9952; found 441.9948.

4.5.7. (E)-5-bromo-N'-((5-bromofuran-2-yl)methylene)-3-phenyl-1H-indole-2-carbohydrazide (27d)

Yellow solid (0.113 g, 0.23 mmol, 79%); R_f 0.5 [EtOAc-Hexane (2:3)]; m.p. 215–218 °C decomposed; ν_{max}/cm^{-1} 3304, 3222, 3054, 2957, 2852, 1738, 1640, 1619, 1258; ^1H NMR (300 MHz, DMSO-d_6) δ 12.19 (s, 1H, CONH), 11.46 (s, 1H, NH), 7.87 (s, 1H, HC = N), 7.73 (br d, J = 1.8 Hz, 1H, H4-ind), 7.50–7.36 (m, 7H, H6-ind, H7-ind, PhH), 6.96 (br s, 1H, H2"-furan), 6.75 (br s, 1H, H3"-furan); ^{13}C NMR (75 MHz, DMSO-d_6) δ 158.19 (C═O), 151.02 (C1"-furan), 135.89 (C═N), 134.39 (C7a-ind), 132.83 (C1′-Ph), 129.55 (C2′-Ph), 128.54 (C3′-Ph), 128.47 (C2-ind), 127.78 (C3a-ind), 126.91 (C4′-Ph), 126.59 (C6-ind), 121.92 (C4-ind), 117.52 (C3-ind), 116.74 (C2"-furan), 114.52 (C7-ind), 114.26 (C3"-furan), 112.96 (C5-ind), C4" *not observed*; HRMS (ESI) *m/z* $[M+H]^+$ calcd for $C_{20}H_{14}O_2N_3^{79}Br_2$ 485.9447; found 485.9437.

4.5.8. (E)-5-fluoro-N'-(furan-2-ylmethylene)-3-phenyl-1H-indole-2-carbohydrazide (27e)

Yellow solid (0.094 g, 0.27 mmol, 75%); R_f 0.5 [EtOAc-Hexane (2:3)]; m.p. 218–221 °C; ν_{max}/cm^{-1} 3307, 3262, 3060, 1644, 1608, 1229; ^1H NMR (300 MHz, DMSO-d_6) δ 12.05 (s, 1H, CONH), 11.34 (s, 1H, NH), 7.94 (s, 1H, H4"-furan), 7.81 (s, 1H, H-C═N), 7.51–7.43 (m, 5H, PhH), 7.33–7.29 (m, 2H, H4-ind, H7-ind), 7.13 (td, J = 9.2, 2.3 Hz, 1H, H6-ind), 6.88 (br s, 1H, H2"-furan), 6.59 (br s, 1H, H3"-furan); ^{13}C NMR (75 MHz, DMSO-d_6) δ 159.27 (d, J = 234.0 Hz, C5-ind), 158.26 (C═O), 149.14 (C1"-furan), 145.35 (C4"-furan), 137.09 (C═N), 133.24 (C1′-Ph), 132.42 (C7a-ind), 129.44 (C2′-Ph), 129.16 (C2-ind), 128.50 (C3′-Ph), 126.73 (C4′-Ph), 126.31 (d, J = 8.9 Hz, C3a-ind), 118.02 (C3-ind), 113.98 (C2"-furan), 113.80 (d, J = 10.1 Hz, C7-ind), 112.83 (d, J = 27.8 Hz, C6-ind), 112.24 (C3"-furan), 104.39 (d, J = 24.1 Hz, C4-ind); ^{19}F NMR (282 MHz, DMSO-d_6) δ −122.72; HRMS (ESI) *m/z* $[M+H]^+$ calcd for $C_{20}H_{15}O_2N_3F$ 348.1143; found 348.1143.

4.5.9. (E)-5-fluoro-N'-((5-methoxyfuran-2-yl)methylene)-3-phenyl-1H-indole-2-carbohydrazide (27f)

Yellow solid (0.078 g, 0.21 mmol, 68%); R_f 0.5 [EtOAc-Hexane (2:3)]; m.p. 185–187 °C; ν_{max}/cm^{-1} 3235, 3026, 2979, 2938, 1615, 1569, 1252; ^1H NMR (300 MHz, DMSO-d_6) δ 12.02 (s, 1H, CONH), 11.16 (s, 1H, NH), 7.72 (s, 1H, H-C═N), 7.49–7.43 (m, 5H, PhH), 7.31–7.28 (m, 2H, H4-ind, H7-ind), 7.12 (br t, J = 8.4 Hz, 1H, H6-ind), 6.81 (br s, 1H, H2"-furan), 5.53 (br s, 1H, H3"-furan), 3.87 (s, 3H, OCH_3); ^{13}C NMR (75 MHz, DMSO-d_6) δ 163.21 (C4"-furan), 159.27 (d, J = 233.5 Hz, C5-ind), 158.02 (C═O), 139.28 (C1"-furan), 136.86 (C═N), 133.31 (C1′-Ph), 132.38 (C7a-ind), 129.45 (C2′-Ph and C2-ind), 128.53 (C3′-Ph), 126.73 (C4′-Ph), 126.36 (d, J = 9.8 Hz, C3a-ind), 117.98 (C2"-furan), 117.64 (C3-ind), 113.78 (d, J = 9.5 Hz, C7-ind), 112.71 (d, J = 26.4 Hz, C6-ind), 104.37 (d, J = 23.7 Hz, C4-ind), 83.08 (C3"-furan), 58.19 (OCH_3); ^{19}F NMR (282 MHz, DMSO-d_6) δ −122.79; HRMS (ESI) *m/z* $[M+H]^+$ calcd for $C_{21}H_{17}O_3N_3F$ 378.1248; found 378.1247.

4.5.10. (E)-N'-((5-chlorofuran-2-yl)methylene)-5-fluoro-3-phenyl-1H-indole-2-carbohydrazide (27g)

Yellow solid (0.087 g, 0.23 mmol, 64%); m.p. 204–207 °C; ν_{max}/cm^{-1} 3221, 3226, 2925, 1617, 1602, 1252; ^1H NMR (300 MHz, DMSO-d_6) δ 12.05 (s, 1H, CONH), 11.43 (s, 1H, NH), 7.86 (s, 1H, H-C═N), 7.51–7.43 (m, 5H, PhH), 7.32–7.28 (m, 2H, H4-ind, H7-ind), 7.13 (td, J = 9.2, 2.4 Hz, 1H, H6-ind), 6.97 (br s, 1H, H2"-furan), 6.62 (br s, 1H, H3"-furan); ^{13}C NMR (75 MHz, DMSO-d_6) δ 159.26 (d, J = 233.7 Hz, C5-ind), 158.30 (C═O), 148.91 (C1"-furan), 137.51 (C═N), 135.87 (C4"-furan), 133.18 (C1′-Ph), 132.45 (C7a-ind), 129.42 (C2′-Ph), 128.98 (C2-ind), 128.48 (C3′-Ph), 126.76 (C4′-Ph), 126.29 (d, J = 10.0 Hz, C3a-ind), 118.15 (C3-ind), 116.40 (C2"-furan), 113.82 (d, J = 9.6 Hz, C7-ind), 112.87 (d, J = 26.0 Hz, C6-ind), 109.47 (C3"-furan), 104.39 (d, J = 23.9 Hz, C4-ind); ^{19}F NMR (282 MHz, DMSO-d_6) δ −122.69; HRMS (ESI) *m/z* $[M+H]^+$ calcd for $C_{20}H_{14}O_2N_3^{35}ClF$ 382.0753; found 382.0753.

4.5.11. (E)-N'-((5-bromofuran-2-yl)methylene)-5-fluoro-3-phenyl-1H-indole-2-carbohydrazide (27h)

Yellow solid (0.098 g, 0.23 mmol, 64%); m.p. 203–207 °C decomposed; ν_{max}/cm^{-1} 3319, 3254, 1649, 1623, 1242; ^1H NMR (300 MHz, DMSO-d_6) δ 12.06 (s, 1H, CONH), 11.43 (s, 1H, NH), 7.86 (s, 1H, H-C═N), 7.51–7.43 (m, 5H, PhH), 7.33–7.29 (m, 2H, H4-ind, H7-ind), 7.14 (td, J = 9.1, 2.4 Hz, 1H, H6-ind), 6.93 (br s, 1H, H2"-furan), 6.72 (br s, 1H, H3"-furan); ^{13}C NMR (75 MHz, DMSO-d_6) δ 159.27 (d, J = 233.9 Hz, C5-ind), 158.33 (C═O), 151.07 (C1"-furan), 135.84 (C═N), 133.17 (C1′-Ph), 132.46 (C7a-ind), 129.43 (C2′-Ph), 129.02 (C2-ind), 128.49 (C3′-Ph), 126.77 (C4′-Ph), 126.28 (d, J = 9.4 Hz, C3a-ind), 124.86 (C4"-furan), 118.14 (C3-ind), 116.67 (C2"-furan), 114.26 (C3"-furan), 113.82 (d, J = 9.4 Hz, C7-ind), 112.89 (d, J = 26.0 Hz, C6-ind), 104.40 (d, J = 23.7 Hz, C4-ind); ^{19}F NMR (282 MHz, DMSO-d_6) δ −122.68; HRMS (ESI) *m/z* $[M+H]^+$ calcd for $C_{20}H_{14}O_2N_3^{79}BrF$ 426.0248; found 426.0247

4.5.12. (E)-5-bromo-N'-(furan-3-ylmethylene)-3-phenyl-1H-indole-2-carbohydrazide (27i)

Yellow solid (0.052 g, 0.13 mmol, 76%); R_f 0.5 [EtOAc-Hexane (2:3)]; m.p. 214–217 °C decomposed; ν_{max}/cm^{-1} 3306, 3238, 3056, 2917, 1643, 1623, 1231; ^1H NMR (300 MHz, DMSO-d_6) δ 12.14 (s, 1H, CONH), 11.29 (s, 1H, NH), 8.11 (br s, 1H, H1"-furan), 8.01 (br s, 1H, H4"-furan), 7.73–7.71 (m, 2H, HC = N, H4-ind), 7.51–6.34 (m, 7H, H6-ind, H7-ind, PhH), 6.77 (br s, 1H, H3"-furan); ^{13}C NMR (75 MHz, DMSO-d_6) δ 158.00 (C═O), 145.75 (C1"-furan), 144.93 (C═N), 140.41 (C4"-furan), 134.32 (C7a-ind), 132.97 (C1′-Ph), 129.58 (C2′-Ph), 128.86 (C2-ind), 128.55 (C3′-Ph), 127.88 (C3a-ind), 126.92 (C4′-Ph), 126.49 (C6-ind), 122.39 (C4-ind), 121.89 (C2"-furan), 117.23 (C3-ind), 114.50 (C7-ind), 112.95 (C5-ind), 107.14 (C3"-furan); HRMS (ESI) *m/z* $[M+H]^+$ calcd for $C_{20}H_{15}O_2N_3^{79}Br$ 408.0342; found 408.0337.

4.5.13. (E)-5-fluoro-N'-(furan-3-ylmethylene)-3-phenyl-1H-indole-2-carbohydrazide (27j)

Yellow solid (0.112 g, 0.32 mmol, 40%); R_f 0.5 [EtOAc-Hexane (2:3)]; m.p. 198–200 °C; ν_{max}/cm^{-1} 3306, 3238, 3056, 2917, 1643, 1623, 1231; ^1H NMR (300 MHz, DMSO-d_6) δ 12.01 (s, 1H, CONH), 11.24 (s, 1H, NH), 8.09 (br s, 1H, H1"-furan), 8.00 (br s, 1H, H4"-furan), 7.71 (s, 1H, H-C═N), 7.50–7.40 (m, 5H, PhH), 7.31–7.27 (m, 2H, H4-ind, H7-ind), 7.11 (td, J = 9.2, 2.3 Hz, 1H, H6-ind), 6.76 (br s, 1H, H3"-furan); ^{13}C NMR (75 MHz, DMSO-d_6) δ 159.26 (d, J = 233.9 Hz, C5-ind), 158.16 (C═O), 145.69 (C1"-furan), 144.90 (C═N), 140.34 (C4"-furan), 133.33 (C1′-Ph), 132.38 (C7a-ind), 129.46 (C2′-Ph), 129.35 (C2-ind), 128.50 (C3′-Ph), 126.73 (C4′-Ph), 126.38 (d, J = 10.3 Hz, C3a-ind), 122.41 (C2"-furan), 117.84 (d, J = 5.2 Hz, C3-ind), 113.79 (d, J = 9.5 Hz, C7-ind), 112.75 (d, J = 29.5 Hz, C6-ind), 107.17 (C3"-furan), 104.36 (d, J = 23.3 Hz, C4-ind); ^{19}F NMR (282 MHz, DMSO-d_6) δ −122.78; HRMS (ESI) *m/z* $[M+H]^+$ calcd for $C_{20}H_{15}O_2N_3F$ 348.1143; found 348.1140.

Declaration of Competing Interest

The authors declare that they have no known competing financial interests or personal relationships that could have appeared to influence the work reported in this paper.

Acknowledgement

I am deeply indebted to the Chulabhorn Royal Academy for the funding support of this project. Also, I would like to express my gratitude to Dr. Pakamas Intachote, Ms. Suchada Sengsai and Ms. Busakorn

Saimanee of the Bioactivity Screening Unit, Chulabhorn Research Institute, for the significant contribution in compound testing in cancer cell lines.

Appendix A. Supplementary material

Supplementary data to this article can be found online at https://doi.org/10.1016/j.bioorg.2021.104795.

References

[1] M.A. Jordan, L. Wilson, Microtubules as a target for anticancer drugs, Nat. Rev. Cancer 4 (4) (2004) 253–265.
[2] R.A. Stanton, K.M. Gernert, J.H. Nettles, R. Aneja, Drugs that target dynamic microtubules: a new molecular perspective, Med. Res. Rev. 31 (3) (2011) 443–481.
[3] J.P. Guastalla 3rd, V. Diéras, The taxanes: toxicity and quality of life considerations in advanced ovarian cancer, Br. J. Cancer 89 (Suppl 3) (2003) S16–S22.
[4] M. Hidalgo, C. Aylesworth, L.A. Hammond, C.D. Britten, G. Weiss, J. Stephenson, G. Schwartz, A. Patnaik, L. Smith, K. Molpus, S. Felton, E. Gupta, K.J. Ferrante, A. Tortora, D.S. Sonnichsen, J. Skillings, E.K. Rowinsky, Phase I and Pharmacokinetic Study of BMS-184476, a Taxane With Greater Potency and Solubility Than Paclitaxel, J. Clin. Oncol. 19 (9) (2001) 2493–2503.
[5] J.A. Garrison, J.S. McCune, R.B. Livingston, H.M. Linden, J.R. Gralow, G.K. Ellis, H. L. West, Myalgias and arthralgias associated with paclitaxel, Oncology (Williston Park, N.Y.) 17 (2) (2003) 271–277, discussion 281-2, 286-8.
[6] E.K. Rowinsky, E.A. Eisenhauer, V. Chaudhry, S.G. Arbuck, R.C. Donehower, Clinical toxicities encountered with paclitaxel (Taxol), Semin. Oncol. 20 (4 Suppl 3) (1993) 1–15.
[7] G.-Z. Li, Y.-H. Hu, D.-Y. Li, Y. Zhang, H.-L. Guo, Y.-M. Li, F. Chen, J. Xu, Vincristine-induced peripheral neuropathy: a mini-review, NeuroToxicol 81 (2020) 161–171.
[8] E.B. Casey, A.M. Jellife, P.M. Le Quesne, Y. Millett, L., Vincristine neuropathy. Clinical and electrophysiological observations, Brain : A J. Neurol. 96 (1) (1973) 69–86.
[9] J.A. Ortega, S.S. Donaldson, S.P. Ivy, A. Pappo, H.M. Maurer, Venoocclusive disease of the liver after chemotherapy with vincristine, actinomycin D, and cyclophosphamide for the treatment of rhabdomyosarcoma. A report of the Intergroup Rhabdomyosarcoma Study Group. Childrens Cancer Group, the Pediatric Oncology Group, and the Pediatric Intergroup Statistical Center, Cancer 79 (12) (1997) 2435–2439.
[10] L. Cooling, M. Bombery, S. Hoffmann, R. Davenport, P. Robertson, J.E. Levine, The impact of recent vincristine on human hematopoietic progenitor cell collection in pediatric patients with central nervous system tumors, Transfusion 54 (8) (2014) 2004–2014.
[11] H.V. Kosmidis, D.O. Bouhoutsou, M.C. Varvoutsi, J. Papadatos, C.G. Stefanidis, P. Vlachos, A. Scardoutsou, A. Kostakis, Vincristine overdose: experience with 3 patients, Pediatr. Hematol. Oncol. 8 (2) (1991) 171–178.
[12] A.A. Ghawanmeh, H.M. Al-Bajalan, M.M. Mackeen, F.Q. Alali, K.F. Chong, Recent developments on (-)-colchicine derivatives: synthesis and structure-activity relationship, Eur. J. Med. Chem. 185 (2020) 111788.
[13] S.N.A. Bukhari, G.B. Kumar, H.M. Revankar, H.-L. Qin, Development of combretastatins as potent tubulin polymerization inhibitors, Bioorg. Chem. 72 (2017) 130–147.
[14] C.M. Abuhaie, E. Bîcu, B. Rigo, P. Gautret, D. Belei, A. Farce, J. Dubois, A. Ghinet, Synthesis and anticancer activity of analogues of phenstatin, with a phenothiazine A-ring, as a new class of microtubule-targeting agents, Bioorg. Med. Chem. Lett. 23 (1) (2013) 147–152.
[15] L. Bohlin, B. Rosen, Podophyllotoxin derivatives: drug discovery and development, Drug Discov. Today 1 (8) (1996) 343–351.
[16] T. Yasmin, H. Zaliha, G. Ahmad Rohi, J. Juriyati, J. Malina, Synthesis of chalcone derivatives and their effects on proliferation and tubulin dynamics instability of HT-29 cells, Lett. Drug Des. Discov. 13 (7) (2016) 662–667.
[17] S. Ducki, Antimitotic chalcones and related compounds as inhibitors of tubulin assembly, Anti-Cancer Agents Med. Chem. 9 (3) (2009) 336–347.
[18] C. Eurtivong, V. Semenov, M. Semenova, L. Konyushkin, O. Atamanenko, J. Reynisson, A. Kiselyov, 3-Amino-thieno[2,3-b]pyridines as microtubule-destabilising agents: Molecular modelling and biological evaluation in the sea urchin embryo and human cancer cells, Bioorg. Med. Chem. 25 (2) (2017) 658–664.
[19] Z.-L. Liu, W. Tian, Y. Wang, S. Kuang, X.-M. Luo, Q. Yu, A novel sulfonamide agent, MPSP-001, exhibits potent activity against human cancer cells in vitro through disruption of microtubule, Acta Pharmacol. Sin. 33 (2) (2012) 261–270.
[20] K. Yoshimatsu, A. Yamaguchi, H. Yoshino, N. Koyanagi, K. Kitoh, Mechanism of action of E7010, an orally active sulfonamide antitumor agent: inhibition of mitosis by binding to the colchicine site of tubulin, Cancer Res. 57 (15) (1997) 3208–3213.
[21] A. Brancale, R. Silvestri, Indole, a core nucleus for potent inhibitors of tubulin polymerization, Med. Res. Rev. 27 (2) (2007) 209–238.
[22] X. Wu, Q. Wang, W. Li, Recent advances in heterocyclic tubulin inhibitors targeting the colchicine binding site, Anti-Cancer Agents Med. Chem. 16 (10) (2016) 1325–1338.
[23] S. Banerjee, K.E. Arnst, Y. Wang, G. Kumar, S. Deng, L. Yang, G.-B. Li, J. Yang, S. W. White, W. Li, D.D. Miller, Heterocyclic-fused pyrimidines as novel tubulin polymerization inhibitors targeting the colchicine binding site: structural basis and antitumor efficacy, J. Med. Chem. 61 (4) (2018) 1704–1718.
[24] J.A. Ecsedy, M. Manfredi, A. Chakravarty, N. D'Amore, Current and next generation antimitotic therapies in cancer, in: D.A. Frank (Ed.), Signaling Pathways in Cancer Pathogenesis and Therapy, Springer, New York: New York, NY, 2012, pp. 5–21.
[25] D.E. Clark, What has virtual screening ever done for drug discovery? Exp. Opin. Drug Discov. 3 (8) (2008) 841–851.
[26] R.V. Guido, G. Oliva, A.D. Andricopulo, Virtual screening and its integration with modern drug design technologies, Curr. Med. Chem. 15 (1) (2008) 37–46.
[27] A.R. Leach, V.J. Gillet, An Introduction to Chemoinformatics, Springer Publishing Company, 2007. Incorporated.
[28] C. Eurtivong, I. Reynisdottir, S. Kuczma, D.P. Furkert, M.A. Brimble, J. Reynisson, Identification of anticancer agents based on the thieno[2,3-b]pyridine and 1H-pyrazole molecular scaffolds, Bioorg. Med. Chem. 24 (16) (2016) 3521–3526.
[29] P. Furet, G. Bold, F. Hofmann, P. Manley, T. Meyer, K.H. Altmann, Identification of a new chemical class of potent angiogenesis inhibitors based on conformational considerations and database searching, Bioorg. Med. Chem. Lett. 13 (18) (2003) 2967–2971.
[30] G.H. Li, J.F. Huang, CDRUG: a web server for predicting anticancer activity of chemical compounds, Bioinformatics 28 (24) (2012) 3334–3335.
[31] J.M. Galúcio, E.F. Monteiro, D.A. de Jesus, C.H. Costa, R.C. Siqueira, G.B.d. Santos, J. Lameira, K.S.d. Costa, In silico identification of natural products with anticancer activity using a chemo-structural database of Brazilian biodiversity, Comput. Biol. Chem. 83 (2019).
[32] F. Kazan, Z.B. Yagci, R. Bai, E. Ozkirimli, E. Hamel, S. Ozkirimli, Synthesis and biological evaluation of indole-2-carbohydrazides and thiazolidinyl-indole-2-carboxamides as potent tubulin polymerization inhibitors, Comput. Biol. Chem. 80 (2019) 512–523.
[33] H.-Z. Zhang, J. Drewe, B. Tseng, S. Kasibhatla, S.X. Cai, Discovery and SAR of indole-2-carboxylic acid benzylidene-hydrazides as a new series of potent apoptosis inducers using a cell-based HTS assay, Bioorg. Med. Chem. 12 (13) (2004) 3649–3655.
[34] G. Jones, P. Willett, R.C. Glen, A.R. Leach, R. Taylor, Development and validation of a genetic algorithm for flexible docking11Edited by F. E. Cohen, J. Mol. Biol. 267 (3) (1997) 727–748.
[35] M.D. Eldridge, C.W. Murray, T.R. Auton, G.V. Paolini, R.P. Mee, Empirical scoring functions: I. The development of a fast empirical scoring function to estimate the binding affinity of ligands in receptor complexes, J. Comput. Aided Mol. Des. 11 (5) (1997) 425–445.
[36] O. Korb, T. Stutzle, T.E. Exner, Empirical scoring functions for advanced protein-ligand docking with PLANTS, J. Chem. Inf. Model. 49 (1) (2009) 84–96.
[37] W.T. Mooij, M.L. Verdonk, General and targeted statistical potentials for protein-ligand interactions, Proteins 61 (2) (2005) 272–287.
[38] M.P. Tantak, L. Klingler, V. Arun, A. Kumar, R. Sadana, D. Kumar, Design and synthesis of bis(indolyl)ketohydrazide-hydrazones: identification of potent and selective novel tubulin inhibitors, Eur. J. Med. Chem. 136 (2017) 184–194.
[39] G. Cihan-Üstündağ, D. Şatana, G. Özhan, G. Çapan, Indole-based hydrazide-hydrazones and 4-thiazolidinones: synthesis and evaluation as antitubercular and anticancer agents, J. Enzyme Inhib. Med. Chem. 31 (3) (2016) 369–380.
[40] D. Kumar, N. Maruthi Kumar, S. Ghosh, K. Shah, Novel bis(indolyl) hydrazide–hydrazones as potent cytotoxic agents, Bioorg. Med. Chem. Lett. 22 (1) (2012) 212–215.
[41] R. Kaur, G. Kaur, R.K. Gill, R. Soni, J. Bariwal, Recent developments in tubulin polymerization inhibitors: an overview, Eur. J. Med. Chem. 87 (2014) 89–124.
[42] C. Jadala, M. Sathish, T.S. Reddy, V.G. Reddy, R. Tokala, S.K. Bhargava, N. Shankaraiah, N. Nagesh, A. Kamal, Synthesis and in vitro cytotoxicity evaluation of β-carboline-combretastatin carboxamides as apoptosis inducing agents: DNA intercalation and topoisomerase-II inhibition, Bioorg. Med. Chem. 27 (15) (2019) 3285–3298.
[43] X.-J. Zhang, Y. Xu, H.-X. Mou, S. Wang, S.-Y. Hao, S.-W. Chen, The synthesis and anti-tumour properties of novel 4-substituted phthalazinones as Aurora B kinase inhibitors, Bioorg. Med. Chem. Lett. 30 (23) (2020) 127556.
[44] D.Y. Shin, H. Sung Kang, G.Y. Kim, W.J. Kim, Y.H. Yoo, Y.H. Choi, Decitabine, a DNA methyltransferases inhibitor, induces cell cycle arrest at G2/M phase through p53-independent pathway in human cancer cells, Biomed. Pharmacother. 67 (4) (2013) 305–311.
[45] F.R. Japp, F. Klingemann, Ueber Benzolazo- und Benzolhydrazofettsäuren, Ber. Dtsch. Chem. Ges. 20 (2) (1887) 2942–2944.
[46] F.R. Japp, F. Klingemann, Zur Kenntniss der Benzolazo- und Benzolhydrazopropionsäuren, Ber. Dtsch. Chem. Ges. 20 (2) (1887) 3284–3286.
[47] F.R. Japp, F. Klingemann, Ueber sogenannte »gemischte Azoverbindungen«, Ber. Dtsch. Chem. Ges. 20 (2) (1887) 3398–3401.
[48] F.R. Japp, F. Klingemann, Ueber die Constitution einiger sogenannten gemischten Azoverbindungen, Justus Liebigs Ann. Chem. 247 (2) (1888) 190–225.
[49] E. Fischer, F. Jourdan, Ueber die Hydrazine der Brenztraubensäure, Ber. Dtsch. Chem. Ges. 16 (2) (1883) 2241–2245.
[50] E. Fischer, O. Hess, Synthese von indolderivaten, Ber. Dtsch. Chem. Ges. 17 (1) (1884) 559–568.
[51] Z. Ju, M. Su, J. Hong, E. La Kim, H.R. Moon, H.Y. Chung, S. Kim, J.H. Jung, Design of balanced COX inhibitors based on anti-inflammatory and/or COX-2 inhibitory ascidian metabolites, Eur. J. Med. Chem. 180 (2019) 86–98.
[52] B. Liu, R. Li, Y. Li, S. Li, J. Yu, B. Zhao, A. Liao, Y. Wang, Z. Wang, A. Lu, Y. Liu, Q. Wang, Discovery of pimprinine alkaloids as novel agents against a plant virus, J. Agric. Food. Chem. 67 (7) (2019) 1795–1806.

[53] V.V. Syakaev, S.N. Podyachev, B.I. Buzykin, S.K. Latypov, W.D. Habicher, A. I. Konovalov, NMR study of conformation and isomerization of aryl- and heteroarylaldehyde 4-tert-butylphenoxyacetylhydrazones, J. Mol. Struct. 788 (1) (2006) 55–62.
[54] M.-C. Sardaru, A.M. Craciun, C.-M. Al Matarneh, I.A. Sandu, R.M. Amarandi, L. Popovici, C.I. Ciobanu, D. Peptanariu, M. Pinteala, I.I. Mangalagiu, R. Danac, Cytotoxic substituted indolizines as new colchicine site tubulin polymerisation inhibitors, J. Enzyme Inhib. Med. Chem. 35 (1) (2020) 1581–1595.
[55] O. Bueno, J. Estévez Gallego, S. Martins, A.E. Prota, F. Gago, A. Gómez-SanJuan, M.-J. Camarasa, I. Barasoain, M.O. Steinmetz, J.F. Díaz, M.-J. Pérez-Pérez, S. Liekens, E.-M. Priego, High-affinity ligands of the colchicine domain in tubulin based on a structure-guided design, Sci. Rep. 8 (1) (2018) 4242.
[56] C.A. Lipinski, F. Lombardo, B.W. Dominy, P.J. Feeney, Experimental and computational approaches to estimate solubility and permeability in drug discovery and development settings, Adv. Drug Deliv. Rev. 23 (1) (1997) 3–25.
[57] D.F. Veber, S.R. Johnson, H.Y. Cheng, B.R. Smith, K.W. Ward, K.D. Kopple, Molecular properties that influence the oral bioavailability of drug candidates, J. Med. Chem. 45 (12) (2002) 2615–2623.
[58] I. Moriguchi, S. Hirono, Q. Liu, I. Nakagome, Y. Matsushita, Simple method of calculating octanol/water partition coefficient, Chem. Pharm. Bull. 40 (1) (1992) 127–130.
[59] N.L. Allinger, Conformational analysis. 130. MM2. A hydrocarbon force field utilizing V1 and V2 torsional terms, J. Am. Chem. Soc. 99 (25) (1977) 8127–8134.
[60] H.M. Berman, J. Westbrook, Z. Feng, G. Gilliland, T.N. Bhat, H. Weissig, I. N. Shindyalov, P.E. Bourne, The protein data bank, Nucl. Acids Res. 28 (1) (2000) 235–242.
[61] A.C. Wallace, R.A. Laskowski, J.M. Thornton, LIGPLOT: a program to generate schematic diagrams of protein-ligand interactions, Protein Eng. 8 (2) (1995) 127–134.
[62] V.A. Vil, G.d.P. Gomes, M.V. Ekimova, K.A. Lyssenko, M.A. Syroeshkin, G. I. Nikishin, I.V. Alabugin, A.O. Terent'ev, Five roads that converge at the cyclic peroxy-criegee intermediates: BF3-catalyzed synthesis of β-hydroperoxy-β-peroxylactones, J. Org. Chem. 83 (21) (2018) 13427–13445.
[63] E. Yasui, M. Wada, N. Takamura, Novel method for synthesis of aryl hydrazones from α-diazo esters: scope and limitations of nucleophiles, Tetrahedron 65 (2) (2009) 461–468.